Combined Analog and Action Potential Coding in Hippocampal Mossy Fibers

Henrik Alle, *et al.*

Science **311**, 1290 (2006);
DOI: 10.1126/science.1119055

Fig. 3. Ras/Raf/MEK/ERK signal transduction pathway and associated genetic syndromes.

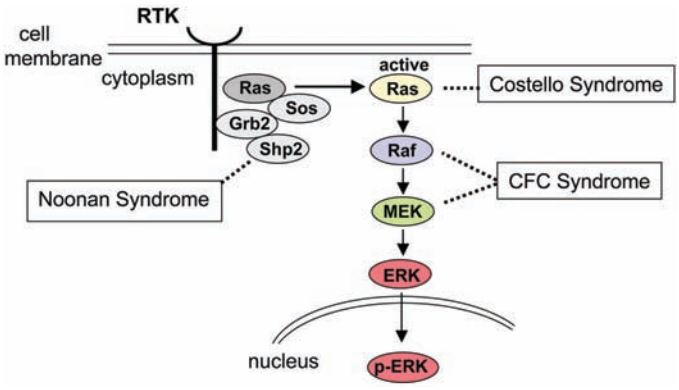

16. A. Bansal, R. D. Ramirez, J. D. Minna, *Oncogene* **14**, 1231 (1997).
17. O. F. Bueno *et al.*, *EMBO J.* **19**, 6341 (2000).
18. R. M. Hobbs, V. Silva-Vargas, R. Groves, F. M. Watt, *J. Invest. Dermatol.* **123**, 503 (2004).
19. F. A. Scholl, P. A. Dumesic, P. A. Khavari, *Cancer Res.* **64**, 6035 (2004).
20. X. Gong *et al.*, *Invest. Ophthalmol. Vis. Sci.* **42**, 539 (2001).
21. J. S. Sebolt-Leopold, R. Herrera, *Nat. Rev. Cancer* **4**, 937 (2004).
22. D. B. Solit *et al.*, *Nature*, published online 6 November 2005 (10.1038/nature04304).
23. We thank CFC International, the families, and donors for their profound contributions; the Genetic Alliance BioBank; and E. Johnson, J. Carey, D. Pinkel, J. Phuchareon, P. Conger, V. St. Pierre, and S. Lee. Supported by NIH grant HD048502 and The Mt. Zion Health Fund (K.A.R.), The Concern and V Foundations (O.T.), and The Durra Foundation and Bristol-Myers Squibb (F.M.).

Supporting Online Material
www.sciencemag.org/cgi/content/full/1124642/DC1
Materials and Methods
Figs. S1 and S2
Tables S1 and S2
References

5 January 2006; accepted 19 January 2006
Published online 26 January 2006;
10.1126/science.1124642
Include this information when citing this paper.

Combined Analog and Action Potential Coding in Hippocampal Mossy Fibers

Henrik Alle and Jörg R. P. Geiger*

In the mammalian cortex, it is generally assumed that the output information of neurons is encoded in the number and the timing of action potentials. Here, we show, by using direct patch-clamp recordings from presynaptic hippocampal mossy fiber boutons, that axons transmit analog signals in addition to action potentials. Excitatory presynaptic potentials result from subthreshold dendritic synaptic inputs, which propagate several hundreds of micrometers along the axon and modulate action potential–evoked transmitter release at the mossy fiber–CA3 synapse. This combined analog and action potential coding represents an additional mechanism for information transmission in a major hippocampal pathway.

The prevailing mode to encode information in the mammalian central nervous system is to convert an analog signal resulting from graded synaptic inputs into patterns of action potentials (APs) (*1*), which are transmitted as all-or-none signals along the axons. By contrast, in primary sensory systems and central neural circuits of small invertebrates, analog signals are used directly to transmit information (*2*, *3*). Comparison of the two modes has revealed that AP coding is less efficient than analog coding at transmitting information (*4*, *5*). Because in many brain regions the axonal distances from the cell body to a large fraction of the corresponding presynaptic boutons are rather short (*6*) and somatic subthreshold signals can be large in amplitude (*7*, *8*), the question arises whether analog axonal signaling contributes to information transmission in the mammalian brain.

To study subthreshold electrical signaling in a cortical presynaptic terminal, we obtained recordings from hippocampal mossy fiber boutons (MFBs) of rats (*9*, *10*) (Fig. 1A). In hippocampal slices at a recording temperature of 34° ± 1°C, extracellular stimulation in the molecular layer of the dentate gyrus (DG-ML) resulted in slow, transient depolarizing voltage deflections at the MFB (Fig. 1B), which we termed excitatory presynaptic potentials (EPreSPs). The peak amplitudes of EPreSPs depended on stimulus intensity in a graded manner (Fig. 1C). Furthermore, EPreSPs exhibited moderate trial-to-trial peak amplitude fluctuations and a slow time course (Fig. 1D). The recorded EPreSPs had a mean peak amplitude of 4.3 ± 0.2 mV and a rise time and a half duration of 20 ± 0.7 ms and 97 ± 3 ms, respectively (n = 49). Underlying currents (EPreSCs) recorded in the voltage-clamp configuration had a peak amplitude of 3.8 ± 0.3 pA, a rise time of 12 ± 1.4 ms, a decay time constant of 46 ± 4 ms, and a half duration of 50 ± 3 ms (n = 10) (Fig. 1D). EPreSP peak amplitudes were reversibly reduced by the bath-applied ionotropic glutamate receptor antagonist 6-cyano-7-nitroquinoxaline-2,3-dione (CNQX) (10 μM) to 0.25 ± 0.02 of control peak amplitudes (n = 6) (Figs. 1E and 2D). Similarly, the selective AMPA receptor antagonist GYKI 53655 (30 μM) reversibly reduced EPreSPs to 0.11 ± 0.03 of control (n = 3) (*11*), indicating that the generation of EPreSPs required AMPA receptor activation.

EPreSPs could be generated either locally in CA3–stratum lucidum (CA3-SL), for example, by heterosynaptic activation of presynaptic ionotropic receptors (*12*, *13*), or remotely as excitatory postsynaptic potentials (EPSPs) at the granule cell dendrites followed by axonal propagation.

Local perfusion of CNQX to the CA3-SL (Fig. 2A) did not significantly reduce the EPreSP peak amplitude compared to control (Fig. 2, B and D) (n = 4, $P > 0.5$), in contrast to the effect of bath application. However, simultaneously recorded field potentials (Fig. 2B) near the MFB recording pipette were reversibly reduced (Fig. 2, B and D) (n = 4, $P < 0.05$), indicating that local drug application was sufficient to block local glutamate receptors. Similarly, local perfusion of tetrodotoxin (TTX) at the hilar end of CA3 (Fig. 2A) resulted in a reversible block of recorded field potentials (0.08 ± 0.05 of control) but attenuated EPreSP amplitudes only slightly, to 0.89 ± 0.04 of control (Fig. 2, C and E) (n = 4, $P < 0.05$). This suggests that EPreSPs were not generated locally in CA3 but represent forward-propagated EPSPs from granule cell dendrites. We consistently found in all post hoc stainings from EPreSP recordings (n = 16) that the corresponding MFB, its axon, and the granule cell soma were anatomically connected (Fig. 3A).

Nonlinear regression analysis of the maximal EPreSP peak amplitudes recorded in MFBs and the respective post hoc determined distances of the recording site to soma revealed a significant correlation (Fig. 3B) (n = 8, $P < 0.05$, and mean distance of 700 μm). Data points were fitted by using a monoexponential function $A_0 \cdot \exp(-\lambda_{EPreSP}/x)$, yielding an average somatic peak depolarization (A_0) of 22 mV and a transient-

Independent Hertie Research Group, Max Planck Institute for Brain Research, D-60528 Frankfurt, Germany.

*To whom correspondence should be addressed. E-mail: geiger@mpih-frankfurt.mpg.de

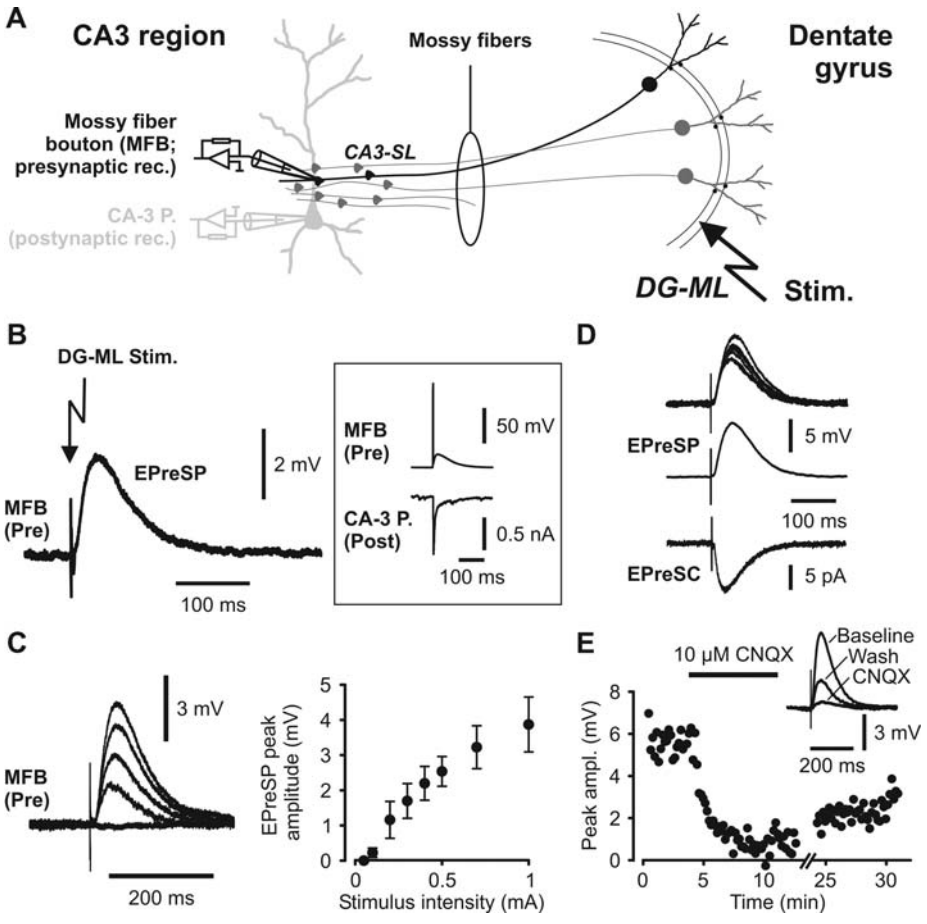

Fig. 1. EPreSPs in MFBs. (**A**) Stimulation and recording configuration. Direct presynaptic recordings from MFBs at 34°C in the CA3-SL and extracellular stimulation (arrow) in the DG-ML. (**B**) (Left) EPreSP recorded from a MFB in the CA3-SL evoked by extracellular stimulation. (Right) A simultaneous recording of the same MFB and a postsynaptic CA3–pyramidal neuron (CA3-P), indicating the functional presynaptic nature of the MFB: top shows MFB AP; bottom, unitary EPSC in CA3-P. (**C**) (Left) EPreSP peak amplitudes depend on stimulus intensity in a graded manner. (Right) Summary of four experiments. (**D**) (Top) Individual EPreSPs superimposed, illustrating the peak amplitude fluctuation of EPreSPs at a fixed stimulus intensity. (Middle) Average EPreSP. (Bottom) Corresponding average EPreSC recorded in the voltage-clamp configuration. (**E**) Reversible reduction of EPreSP amplitude by AMPA and kainate antagonist CNQX (10 μM, bath application). (Inset) Corresponding average EPreSPs.

signal space constant (λ_{EPreSP}) of 430 μm. EPSPs of comparable amplitude (up to 35 mV) were recorded from granule cell somata upon stimulation in DG-ML (fig. S1) because granule cells in the dentate gyrus exhibit negative resting potentials close to –80 mV (fig. S1) (n = 16). Similar EPSP amplitudes and resting potentials were reported both in vitro (*14*, *15*) and in vivo (*16*, *17*).

To relate amplitude and shape of somatic EPSPs and EPreSPs, we developed a passive compartmental model of a schematized granule cell including axon and MFBs based on realistic morphology (*10*) and passive membrane properties (fig. S2). The model reproduced experimentally determined parameters like membrane time constant τ_0 (62 ± 4 ms, n = 10) (Fig. 3C), mossy fiber input resistance (1.4 ± 0.1 GΩ, n = 31), and MFB capacitance (*9*, *18*).

The constrained model reproduced the experimentally determined distance dependence of EPreSP peak amplitude, yielding a λ_{EPreSP} of about 450 μm. The axonal steady state space constant from model simulations was estimated to be around 700 μm (fig. S2), which is larger than expected from previous mossy fiber modeling (*19*) but very similar to values found in the posterior pituitary (*20*).

Simulated somatic EPSPs and measured granule cell EPSPs had half durations of 39 ms and 36 ± 2 ms (n = 10), respectively (figs. S1 and S2). Simulated EPreSPs (at 750 μm) and measured EPreSPs (mean distance to the soma of 700 μm) had half durations of 84 ms and 99 ± 10 ms (n = 8), respectively (Fig. 1 and fig. S2). Thus, the slow time course of EPreSPs can be explained by axonal filtering during passive propagation.

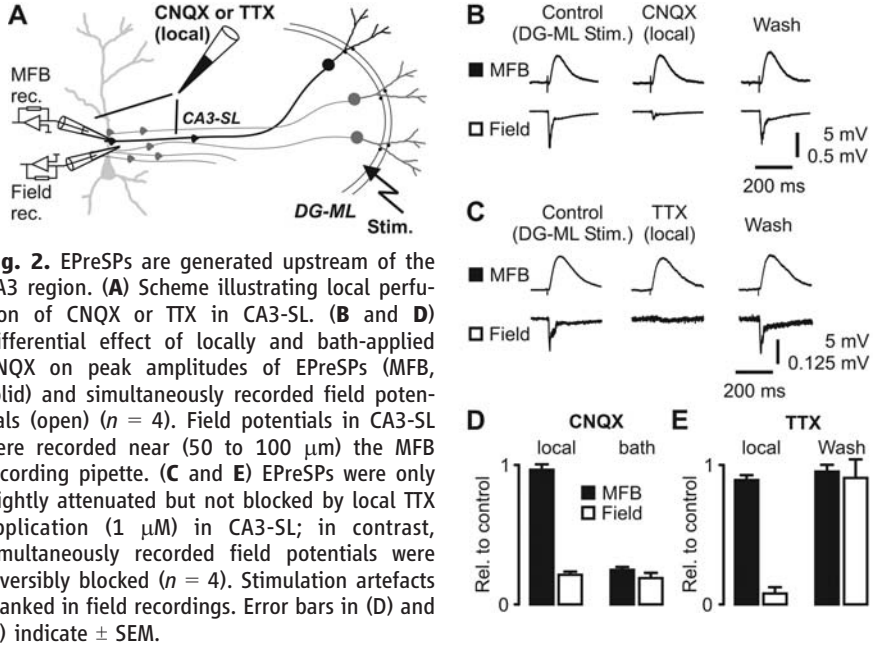

Fig. 2. EPreSPs are generated upstream of the CA3 region. (**A**) Scheme illustrating local perfusion of CNQX or TTX in CA3-SL. (**B** and **D**) Differential effect of locally and bath-applied CNQX on peak amplitudes of EPreSPs (MFB, solid) and simultaneously recorded field potentials (open) (n = 4). Field potentials in CA3-SL were recorded near (50 to 100 μm) the MFB recording pipette. (**C** and **E**) EPreSPs were only slightly attenuated but not blocked by local TTX application (1 μM) in CA3-SL; in contrast, simultaneously recorded field potentials were reversibly blocked (n = 4). Stimulation artefacts blanked in field recordings. Error bars in (D) and (E) indicate ± SEM.

To prove experimentally that depolarization of granule cell dendrites is sufficient to substantially depolarize MFBs in CA3-SL, we puff-

applied focally 1 mM RS-AMPA in the DG-ML after blocking synaptic transmission (Fig. 3, A and D). The average AMPA-mediated depolarization at MFBs was 7.7 ± 0.4 mV (n = 5) and, in the presence of TTX (0.5 μM), 6.1 ± 0.8 mV (n = 4) (Fig. 3D; somatic responses, fig. S1), demonstrating passive propagation of subthreshold depolarizations to MFBs (Fig. 3D).

The propagation of depolarizing signals raises the question of whether hyperpolarizing signals also propagate. The negative resting membrane potential of granule cells does not favor the generation of large-amplitude hyperpolarizations at the soma under the experimental conditions used. However, it is conceivable that hyperpolarizing potentials propagate when generated by inhibitory inputs during depolarized membrane potential states, as observed in vivo (*7*).

To address the functional importance of transient subthreshold depolarizations, we first studied the interaction of EPreSPs and presynaptic APs. APs recorded in MFBs were elicited by stimulation in DG-ML. A comparison of APs in isolation with APs of an EPreSP-AP combination, which was evoked by a double stimulation (at subthreshold and suprathreshold intensity, separated by 50 ms), did not reveal a detectable difference in AP shape (n = 4) (Fig. 4, A and C). Even steady state depolarizations of comparable amplitude caused only little changes in AP shape (fig. S3). Second, to test whether EPreSPs change presynaptic calcium signaling, we performed presynaptic voltage-clamp experiments to analyze the presynaptic calcium current underlying waveforms of an AP, an EPreSP, and a combination of both. Consistent with the properties of presynaptic calcium channels in MFBs (*21*), no calcium current was detectable during EPreSP waveforms, and calcium transients did not differ between waveforms of the AP and those of the combination of EPreSP and AP (n = 6) (Fig. 4, B and C). Third, we compared three presynaptic conditions in paired recordings from MFBs and postsynaptic CA3 neurons. In contrast to APs, EPreSPs (evoked by local injection of an EPreSC waveform) did not elicit a detectable signal in the postsynaptic neuron (Fig. 4D), but the combination of EPreSPs and APs (APs 10 to 20 ms after the peak of the EPreSPs) evoked markedly larger average excitatory postsynaptic currents (EPSCs) in the postsynaptic neuron than did APs alone (1.43 ± 0.09 of unconditioned trials, n = 11, P < 0.005) (Fig. 4, D and E), indicating that EPreSPs enhance AP-evoked transmitter release. The EPreSP enhancement of EPSCs was less pronounced when APs were timed in the late decay phase or in the late period of a nondecaying EPreSP (fig. S4).

In paired recordings using 10 mM of the calcium chelator EGTA in the presynaptic recording solution, we still found EPreSP enhancement of EPSCs (1.21 ± 0.04, n = 5, P < 0.05) (Fig. 4E), but the extent was attenuated (10 mM EGTA versus control, P = 0.06). Therefore, the extent of EPreSP enhancement of EPSCs seems to depend on background calcium signaling, but our results are also consistent with a partial direct voltage modulation of release machinery, suggesting a different transduction mechanism of subthreshold signals at the MFB than that found at the calyx of Held (*22*).

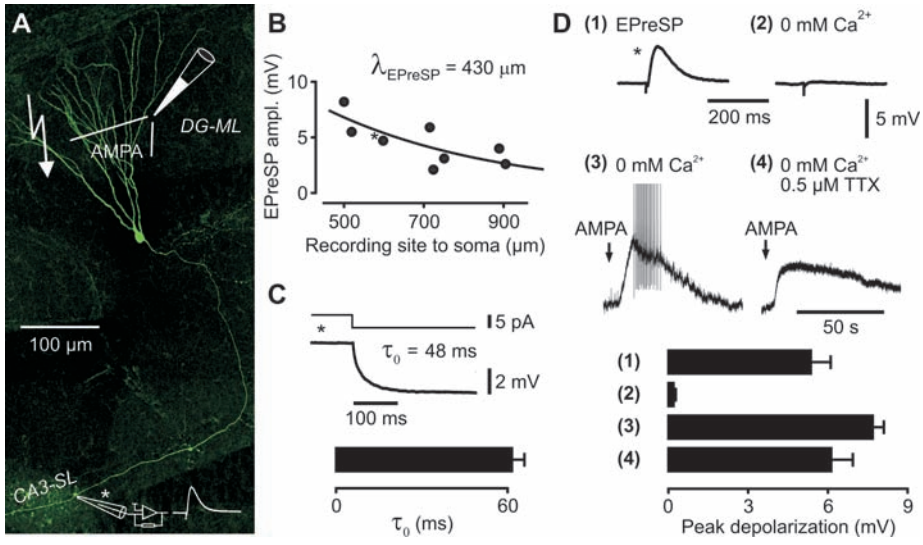

Fig. 3. Propagation of somatic depolarizations underlies EPreSPs. (**A**) Post hoc confocal image of a granule cell filled with biocytin during a MFB recording. Schematic patch pipette indicates recording site. Schematic pipette in DG-ML indicates site of AMPA puff application. (**B**) Maximal EPreSP peak amplitude of individual experiments correlated with distance of recording site to granule cell soma (P < 0.05, n = 8); monoexponential fit curve superimposed. (**C**) Mossy fiber steady state membrane τ_0 was estimated from hyperpolarizing pulses (for bar graph, n = 10). (**D**) Propagation of dendritic depolarization to MFBs. Step 1: EPreSP evoked in a MFB. Step 2: Block of synaptic transmission (modified artificial cerebrospinal fluid: 0 mM Ca^{2+}, 3 mM Mg^{2+}). Step 3: Focal AMPA puff application in DG-ML evoked a transient depolarization at the MFB in combination with APs (see fig. S1 for somatic AMPA puff responses). Step 4: Additional TTX (0.5 μM) abolished APs. Bars in the lower part summarize the mean peak depolarizations at the MFBs caused by the sequence of conditions 1 to 4 shown in the upper part of (D) (n either 4 or 5). Asterisks in (A) to (D), traces 1 to 4, mark measurements of the same MFB recording. Error bars, ± SEM.

In vivo, large amplitude theta oscillations (20 mV) in combination with APs have been described in granule cells (*7*). Subthreshold oscillations of such amplitude are likely to be propagated to presynaptic terminals (fig. S2). Therefore, we compared postsynaptic responses to APs (three APs at 5 Hz) with and without presynaptic subthreshold theta-like oscillations (5 Hz) in paired recordings (Fig. 4, F and G). Presynaptic subthreshold theta oscillations enhanced EPSCs while preserving multiple pulse facilitation (*23*) (Fig. 4G). This suggests a general functional role of subthreshold membrane potential changes to the regulation of synaptic transmission during naturally occurring activity patterns of granule cells (*24*). A similar function of subthreshold oscillations for synaptic output was found in invertebrates (*25*, *26*).

In conclusion, the output information of hippocampal granule cells is not exclusively encoded in the number and timing of APs. The combined analog and AP coding reported here is likely to enhance information capacity of synapses and may increase the computational power of the dentate gyrus–CA3 network.

References and Notes

1. F. Rieke, D. Warland, R. De Ruyter van Steveninck, W. Bialek, *Spikes: Exploring the Neuronal Code* (Bradford MIT Press, Cambridge, MA, 1998).
2. V. M. Pasztor, B. M. H. Bush, *Science* **215**, 1635 (1982).
3. M. Juusola, A. S. French, R. O. Uusitalo, M. Weckström, *Trends Neurosci.* **19**, 292 (1996).
4. R. R. De Ruyter van Steveninck, S. B. Laughlin, *Nature* **379**, 642 (1996).
5. M. Juusola, A. S. French, *Neuron* **18**, 959 (1997).
6. R. J. Douglas, C. Koch, M. Mahowald, K. A. C. Martin, H. H. Suarez, *Science* **269**, 981 (1995).
7. M. D. Munoz, A. Nunez, E. Garcia-Austt, *Brain Res.* **509**, 91 (1990).
8. C. C. H. Petersen, T. T. G. Hahn, M. Mehta, A. Grinvald, B. Sakmann, *Proc. Natl. Acad. Sci. U.S.A.* **100**, 13638 (2003).
9. J. R. P. Geiger, P. Jonas, *Neuron* **28**, 927 (2000).
10. L. Acsady, A. Kamondi, A. Sik, T. Freund, G. Buzsaki, *J. Neurosci.* **18**, 3386 (1998).
11. H. Alle, J. R. P. Geiger, unpublished data.
12. D. Schmitz, J. Mellor, R. A. Nicoll, *Science* **291**, 1972 (2001); published online 8 February 2001 (10.1126/science.1057105).
13. A. Ruiz *et al.*, *Neuron* **39**, 961 (2003).
14. K. J. Staley, T. S. Otis, I. Mody, *J. Neurophysiol.* **67**, 1346 (1992).
15. C. Schmidt-Hieber, P. Jonas, J. Bischofberger, *Nature* **429**, 184 (2004).
16. M. Penttonen, A. Kamondi, A. Sik, L. Acsady, G. Buzsaki, *Hippocampus* **7**, 437 (1997).
17. T. M. Gao, E. M. Howard, Z. C. Xu, *J. Neurophysiol.* **80**, 2860 (1998).
18. S. Hallermann, C. Pawlu, P. Jonas, M. Heckmann, *Proc. Natl. Acad. Sci. U.S.A.* **100**, 8975 (2003).

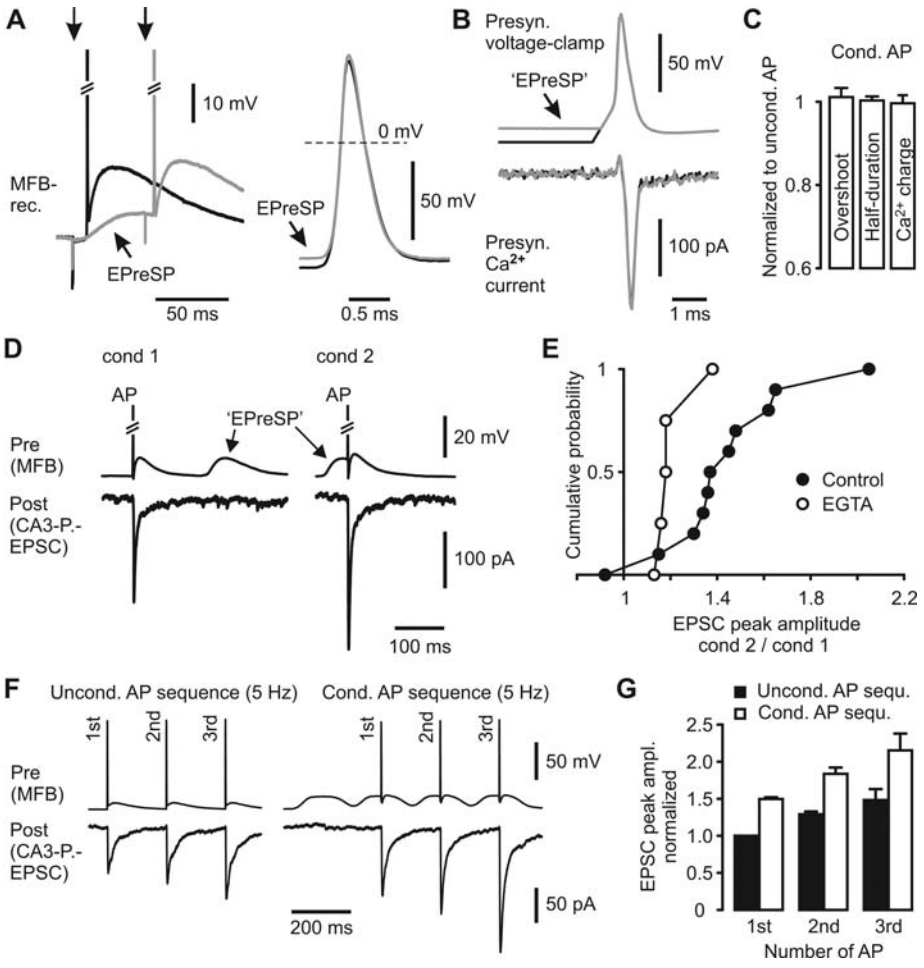

Fig. 4. EPreSPs enhance AP-evoked transmitter release. (**A**) MFB recording and stimulation in DG-ML (arrows). (Left) An AP (black trace) was elicited by suprathreshold stimulation; an EPreSP-AP sequence (gray trace) was evoked by a subthreshold followed by a suprathreshold stimulation (50-ms interval). (Right) APs superimposed. (**B**) (Top) AP and EPreSP-AP waveforms used as voltage commands in MFBs. (Bottom) Evoked presynaptic calcium currents. (**C**) Summary bar graph of experiments in (A) (n = 4) and (B) (n = 6). (**D**) Paired recordings (both AP and EPreSP were evoked by current injection into the MFB). The MFB-AP (top traces) was alternately elicited before the EPreSP (cond 1) or briefly after the peak of the EPreSP (cond 2). Bottom traces, average unitary EPSCs. (**E**) Cumulative distribution of EPSC peak amplitude ratio (cond 2/cond 1). For controls, n = 11; for 10 mM EGTA in the presynaptic pipette, n = 5. (**F**) Subthreshold theta-like oscillations modify synaptic transmission. Upper traces: left, presynaptic unconditioned AP sequence (5 Hz); right, AP sequence conditioned by theta-like oscillations. Bottom traces, average EPSCs. (**G**) Summary bar graph of experiments in (F) (n = 4). All EPSCs were normalized to the first EPSC of the unconditioned AP sequence. Error bars, ± SEM.

19. D. Engel, P. Jonas, *Neuron* **45**, 405 (2005).
20. M. B. Jackson, *J. Neurophysiol.* **69**, 692 (1993).
21. J. Bischofberger, J. R. P. Geiger, P. Jonas, *J. Neurosci.* **22**, 10593 (2002).
22. G. B. Awatramani, G. D. Price, L. O. Trussell, *Neuron* **48**, 109 (2005).
23. P. A. Salin, M. Scanziani, R. C. Malenka, R. A. Nicoll, *Proc. Natl. Acad. Sci. U.S.A.* **93**, 13304 (1996).
24. W. E. Skaggs, B. L. McNaughton, M. A. Wilson, C. A. Barnes, *Hippocampus* **6**, 149 (1996).
25. A. I. Ivanov, R. L. Calabrese, *J. Neurosci.* **23**, 1206 (2003).
26. P. S. Katz, *Curr. Biol.* **13**, R554 (2003).

27. We thank F. Tennigkeit for discussion; M. Häusser, A. Roth, T. Ishikawa, and G. Pipa for reading an earlier version of the manuscript; and I. Wüllenweber for technical assistance. This work was supported by the Hertie Foundation, the Deutsche Forschungsgemeinschaft, and the Max Planck Society.

Supporting Online Material

www.sciencemag.org/cgi/content/full/311/5765/1290/DC1
Materials and Methods
Figs. S1 to S4

18 August 2005; accepted 27 January 2006
10.1126/science.1119055

Chemical Rescue of a Mutant Enzyme in Living Cells

Yingfeng Qiao,[1] Henrik Molina,[2] Akhilesh Pandey,[2] Jin Zhang,[1] Philip A. Cole[1]*

The restoration of catalytic activity to mutant enzymes by small molecules is well established for in vitro systems. Here, we show that the protein tyrosine kinase Src arginine-388→alanine (R388A) mutant can be rescued in live cells with the use of the small molecule imidazole. Cellular rescue of a viral Src homolog was rapid and reversible and conferred predicted oncogenic properties. Using chemical rescue in combination with mass spectrometry, we confirmed six known Src kinase substrates and identified several new protein targets. Chemical rescue data suggest that cellular Src is active under basal conditions. Rescue of R388A cellular Src provided insights into the mitogen-activated protein kinase pathway. This chemical rescue approach will likely have many applications in cell signaling.

Elegant studies have established the utility of chemical complementation in the analysis of ligand-receptor and enzyme-inhibitor interactions in cellular systems (*1*–*3*). These approaches allow highly specific and precise temporal control of cellular pathways. Complementation of enzymes containing active-site mutations has involved functional substitution of the missing side chain with a small compound that possesses similar electronic or steric features (*4*–*6*). The obstacles to in vivo application include the requirement for a cell-permeable and relatively nontoxic small-molecule rescue agent. It was shown recently that when Arg^{318} in Csk (a conserved residue in tyrosine kinases) was mutated to Ala, it could be effectively rescued by imidazole (*7*). An actin stress fiber assay in fibroblasts suggested that R318A Csk might be rescuable in living cells (*8*). However, the maximal level of rescue was 5% of wild-type activity and this together with incomplete cellular characterization led to uncertainty in these findings.

We investigated chemical rescue with the nonreceptor protein tyrosine kinase Src. Src, the